Check for updates

ADVANCED MATERIALS TECHNOLOGIES
www.advmattechnol.de

Propulsion of Magnetic Beads Asymmetrically Covered with DNA Origami Appendages

*Christoph Pauer, Aron Venczel, Mihir Dass, Tim Liedl, and Joe Tavacoli**

Eukaryotic cells that swim by the beating of nanoscale elastic filaments (flagella) present a promising locomotion paradigm for man-made analogues essential for next-generation in-vivo treatments and for the study of collective phenomena at the low Reynolds number limit. However, artificial analogues have been limited to many microns in size due to the engineering challenges of fabricating actable flexible filaments at the nanoscale—thereby narrowing the application scope. Here, made-to-order nanoscale filaments designed on the molecular level are fabricated using the DNA-origami technique. It is found that magnetic beads anisotropically covered with such bundles move in a ballistic fashion when wagged back and forth under an external magnetic field. Furthermore, by comparing bead dynamics at a range of bundle coverages and driving frequencies, compelling evidence is amassed to suggest that this ballistic motion is imparted by the beating of the DNA origami filaments as synthetic flagella. This proof-of-concept work opens up avenues for further made-for-purpose appendages designed using DNA self-assembly and with it ever more complex locomotion on the nano and microscale.

1. Introduction

The research on synthetic self-propelled microscale locomotors, or synthetic micromotors, is fast-expanding due to the potential of these devices for in/ex vivo drug and gene delivery, diagnostics, mechanical action and as platforms to research the physics of collective motion in the absence of biological complications.[1–11] Synthetic micromotors can be divided into two subsets: those driven by external fields (magnetic, electrical, light, ultrasound etc.) and those using fuel for propulsion.[2,5,12–16] Magnetically driven micromotors are especially attractive because of their price, biocompatibility, capacity for adaptive propulsion and for long-range autonomy suitable for deep function within the body.[16–24] Indeed, magnetic fields are particularly useful for imparting beating and/or rotating actuation to micromotors that mimic biological microswimmers. The seminal example is a swimmer built by Dreyfus et al. consisting of a string of magnetic beads tethered to a red blood cell.[25] Here, swimming is induced in a derivative manner to sperm, that is, by beating a flexible appendage that supports the propagation of a bending wave. Since this breakthrough, several other bioinspired magnetic microswimmers have been fabricated, including those made from custom-made micromagnets, soft-magnetic composites and numerous architectures in which a magnetic region actuates nonmagnetic flagella/appendages.[13,15,16,20,26–29] Increasingly, the role of appendage architecture on swimming performance is being investigated, demonstrating that swimming speed varies with its length, elasticity, and stroke frequency for both biological and synthetic systems.[15,26,28,30] Furthermore, it has been established that collective interactions of biological microswimmers are delicately dependent depend delicately on coupled flagellar (appendage) dynamics and flows generated at sub-flagellum length scales.[30] These interactions are exploited in nature to facilitate performance: mice sperm, for instance, form long trains that enhance their velocity.[7,10,30–33] Nevertheless, rigorous control of appendage design for synthetic systems remains taxing, even more so when nanoscale features are required. A particularly promising approach to achieving such control on the nanoscale is DNA self-assembly, as employed by Maier et al. to generate synthetic flagella based on DNA tile-tube bundles.[26] When attached to rotating magnetic beads, these bundles hydrodynamically assembled into a corkscrew-like confirmation of several micrometers to drive translational motion in a manner analogous to bacteria. Though the assembly technique permitted exquisite control of twist and stiffness of the synthetic flagella, their length was subject to oligomerization and uncontrolled. In this communication we build on the work of Maier et al. by using an alternative DNA self-assembly strategy, DNA origami. Here a single-stranded DNA loop of 8634 nucleotides is folded in a predetermined manner by the specific binding of single-stranded DNA oligomers to build bespoke, nanoscale appendages of controlled dimension.[34–37] We present a method to modulate the coverage of our appendages onto magnetic beads uniformly or with broken symmetry. On rocking these constructs via a time-dependent magnetic field, we find that while architectures fully covered with the DNA origami exhibit largely Brownian kinetics,

C. Pauer, A. Venczel, M. Dass, T. Liedl, J. Tavacoli
Faculty of Physics and Center for NanoScience
Ludwig-Maximilians-Universität
Geschwister-Scholl-Platz 1 80539, München, Germany
E-mail: j.tavacoli@lmu.de

The ORCID identification number(s) for the author(s) of this article can be found under https://doi.org/10.1002/admt.202200450.

© 2022 The Authors. Advanced Materials Technologies published by Wiley-VCH GmbH. This is an open access article under the terms of the Creative Commons Attribution License, which permits use, distribution and reproduction in any medium, provided the original work is properly cited.

DOI: 10.1002/admt.202200450

symmetry broken architectures i.e. beads partially covered with DNA origami, move in a ballistic manner consistent with a swimming mechanism. Finally, we realize directionality into our swimmers upon assembly by introducing a constant magnetic field during the grafting procedure, thereby advancing these constructs toward controlled delivery application on the microscale.

2. Results and Discussion

The foundation of our synthetic appendages is a six helix-bundle (6HB) DNA origami.[38–40] These bundles have a defined length (≈490 nm), thickness (6–8 nm) and persistence length (1.88–2.7 µm).[39] Moreover, we note that in comparison to DNA tile-tubes, and more generally, the bundles are a well-established design that may be robustly assembled at high yields, controllably oligomerized end-to-end and functionalized at predetermined sites to direct their binding to external functional groups of choice and are a platform with significant design space for future performance optimization.[38,39] These factors make them ideal proof-of-concept DNA origami geometries to act as slender bodies for low Reynolds number propulsion. Indeed, such types of bundles have already shown suitability for controlled micron-scale actuation on application of electric fields and when tethered to magnetic particles and have also been carried by gold nanoparticles in thermophoretic flows.[41–45] As actuating units, we use streptavidin-covered magnetic Beads (MyOne, streptavidin T1, diameter = 1 µm) that experience torque if their magnetic easy axis is misaligned to an external magnetic field.[46,47] By functionalizing one end of our 6HBs with biotin we exploit the streptavidin-biotin interaction to attach them to the surface of the magnetic beads, with the long axis of the bundles on average directed outward from the surface of the bead. We undertake grafting with the beads positioned in three distinct settings: 1) in bulk, that is, the beads fully dispersed, 2) the beads resting on a flat interface and 3) with the beads partially sitting within PDMS microwells. Using these distinct grafting environments, we can adjust the grafting coverage to fabricate beads fully covered with 6HBs (FC beads, setting 1), beads predominately covered with bundles (PC beads, setting 2) and beads hemispherically covered with bundles (HC beads, setting 3) (**Figure 1**a). For clarity, whereas the FC

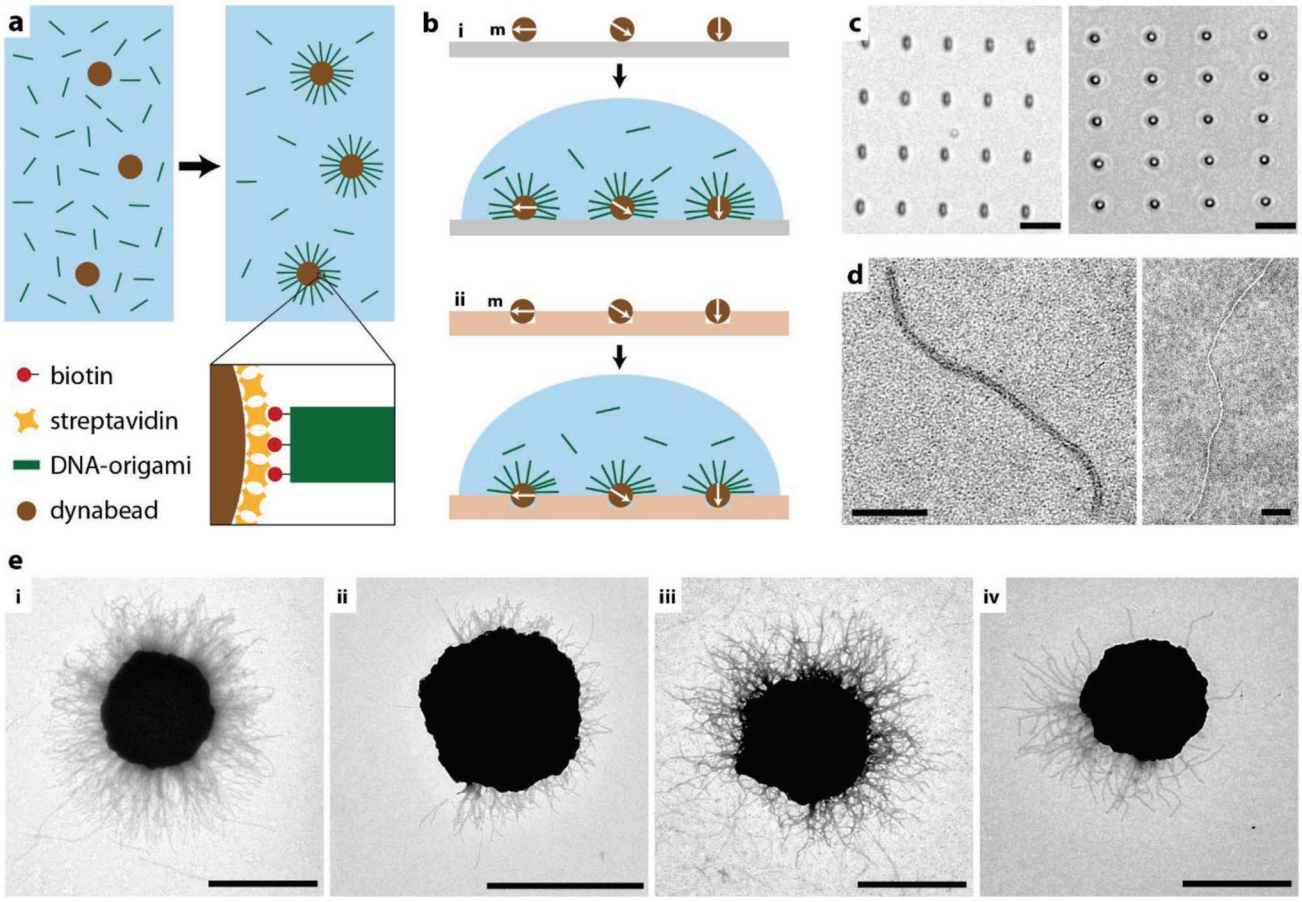

Figure 1. The grafting of biotin-capped DNA origami 6HBs onto streptavidin-functionalized magnetic beads. a) Grafting took place in bulk, b.i) on a flat glass substrate, and ii) trapped in PDMS microwells to produce fully covered (FC) beads, predominately covered beads (PC) beads and hemispherically covered (HC) beads, respectively. In addition, PC beads grafted with 6HB monomers were prepared (PCM). c) Bright-field microscopic images of a PDMS mold used for the preparation of HC beads, empty (left) and populated with native beads (right). Scale bars: 5 µm. d) TEM micrographs of a 6HB monomer (left) and dimer (right). Scale bars are 100 nm. e) TEM micrographs of i) FC beads, ii) PCM beads, iii) PC beads, and iv) HC beads (6HB dimers). Scale bars: 1 µm.

© 2022 The Authors. Advanced Materials Technologies published by Wiley-VCH GmbH

2365709x, 2022, 12, Downloaded from https://onlinelibrary.wiley.com/doi/10.1002/admt.202200450 by Cochrane Germany, Wiley Online Library on [29/09/2023]. See the Terms and Conditions (https://onlinelibrary.wiley.com/terms-and-conditions) on Wiley Online Library for rules of use; OA articles are governed by the applicable Creative Commons License

beads have an isotropic architecture, the PC and HC beads sets are inherently symmetry-broken designs, with the HC design being the most sparsely covered. We make 6HB dimers (end-to-end length ≈ 1 μm) by coupling 6HB monomers tip-to-tip using complementary base pair interactions (so-called 'sticky ends') and bind them to the beads in all of the grafting scenarios. In contrast to the dimer configuration, we also prepare PC beads populated with monomers of 6HB (PCM). We employ a time-varied transverse magnetic field in the x–y plane to rock our beads back and forth around a fixed axis in the z-plane. We adjust the frequency, f, of the field and track the motion of individual beads sedimented to the base of an enclosed cell. For a population of beads, we extract the magnitude of a mean velocity, v, by fitting a mean square displacement to a function incorporating both Brownian and ballistic dynamics (**Figure 2**, refer to Section S1, Supporting Information).[48] In doing so, we find that the PC and HC bead populations move ballistically in random orientations, characterized by f–v curves with a mean velocity maximum at intermediate frequencies on the order of 100 nm s^{-1} (Figure 2a-i,iii,iv,b). In contrast, the FC beads (and native Dyna beads and FCM system (Section S2, Supporting Information)) show only Brownian dynamics when subject to the imposed time-varied magnetic field, resulting in a flat f–v curve (Figure 2a-ii,c). This distinction between symmetry-broken bead architectures and isotropic ones is revealing. It strongly infers that the ballistic motion of the former is not a consequence of flow, magnetic field gradients, biased rolling, or any intrinsic property of the DNA origami bundles. Instead, the motion is most consistent with the bundles acting as flexible appendages that create thrust by supporting a bending wave generated by the oscillation of the magnetic beads, that is, swimming. Such a swimming mechanism parallels the sinusoidal whip-like motion of sperm flagella. Indeed, this method of propulsion is compatible with the baseline physics of our system; for the 6HBs to induce effective locomotion via a bending wave, the elastic and drag forces acting on them must be well matched. We estimate a viscous-elastic force ratio from 1–10 for the frequency range of our experiments (Section S3, Supporting Information), values associated with efficient swimming at low Reynolds number.[25,49,50] To further certify this mode of transport, we adjust the amplitude of the oscillating field at 50 Hz, and with it the amplitude of bead rocking, to extract PC bead velocity for a single micromotor. We find that the bead's velocity increases monotonically with amplitude, consistent with the velocity scaling of a bending wave at a fixed wavelength (Section S3, Supporting Information).[51]

Swimming via appendage beating also offers a rationale for the key features of our experiments. For instance, we can understand the non-ballistic activity of the FC beads in terms of zero net-thrust creation as any propulsive forces generated would isotropically emanate outward via the corona of bundles. In contrast, the symmetry broken architectures would produce net thrust aligned and opposite with the 6HB orientation and consequently move ballistically, as observed. The random direction of their paths then results from the arbitrary orientation of the bundles with respect to the beads' magnetic easy axis; though the latter orientate with the direction of the fluctuating magnetic field, the bundles do not. Propulsion will therefore be generated in a range of directions. Derivatives of these arguments, albeit qualitatively, also explain the top velocities reached by HC beads, PCM beads and PC beads: ≈300 nm s^{-1}, ≈200 nm s^{-1} and ≈120 nm s^{-1} respectively (Figure 2a). The highest velocity of the HC beads can be rationalized by noting a greater portion of its 6HBs can create thrust in the same direction in comparison to the PC beads, where many of the bundles will work opposingly to lower the net-thrust-to-drag ratio. The intermediate velocity of the PC monomer system is then consistent with a reduced drag acting on the bead (due to its shorter bundles) than the PC dimer design.

In addition, we mention that the maxima form of the f–v curves is consistent with data reported on other synthetic microswimmers employing a beating stroke. In these cases, the peak velocities at intermediate frequencies reflect the optimal balance of efficient stroke form and beating frequency.[15,25,49,50] However, a full analysis of our curves must not only account for the length, coverage and density of the bundles on the beads, but also their frequency sensitive stroke patterns and the nature of bead actuation with frequency.[47] Such an analysis is beyond the scope of this communication, being the subject of ongoing theoretical work. Nevertheless, from a practical perspective, the curves demonstrate that one can use field frequency to select for an average velocity of choice. For the HC beads, we can choose between limits of 80–250 nm s^{-1} within the frequency range of our experiments. Beyond mechanistic understanding, it is also evident that we have realized the first DNA origami-based micromotors. Purely ballistic micromotors have demonstrated effective active-agent delivery on the microscale.[52]

Because external fields drive our micromotors, we can trigger their activity on and off. **Figure 3**a displays this situation for the HC beads, where their reversible transfer from Brownian to ballistic dynamics is evident. The same figure also highlights some nuances in the motion of our microdevices. For instance, we observe an occasional $|\pi|$ switch in their trajectory on removing and reapplying the external field. This directional switch most likely arises from the magnetic beads' known π periodicity of magnetic symmetry and its coupling to a Brownian rotation $> |½\ \pi|$ during the beads' field-off periods.[46] We also notice a prevalence of short-lived $|½\ \pi|$ changes in directions. This behavior is harder to account for. We cautiously suggest its relation to a theorized $|½\ \pi|$ flip in the magnetization vector when the phase lag between the time-varied field and the easy axis of magnetization approaches $|¼\ \pi|$—but further investigation is required to understand this phenomenon.

Figure 3a additionally demonstrates (along with the error bars for f–v plots) that whilst, on average, the PC and HC beads have a clear signature of ballistic motion, significant variability in their displacements, i.e. swimming velocities, exist for given frequencies. Most dramatically, in the case of the HC population driven at 80 Hz, the fastest individual swimmer attains a velocity close to 1 μm s^{-1}, whereas the motion of the slowest of the same population can be attributed to thermal noise alone (Section S4, Supporting Information). A portion of this heterogeneity of performance undoubtedly stems from our magnetic beads: magnetic torsional stiffness differences of as much as 30% have been reported for those employed here, attributed to subtle variations in the distribution, shape and size of their iron oxide content.[46] Consequently, seemingly equivalent beads may be optimally driven at distinct frequencies.[47]

© 2022 The Authors. Advanced Materials Technologies published by Wiley-VCH GmbH

2365709x, 2022, 12, Downloaded from https://onlinelibrary.wiley.com/doi/10.1002/admt.202200450 by Cochrane Germany, Wiley Online Library on [29/09/2023]. See the Terms and Conditions (https://onlinelibrary.wiley.com/terms-and-conditions) on Wiley Online Library for rules of use; OA articles are governed by the applicable Creative Commons License

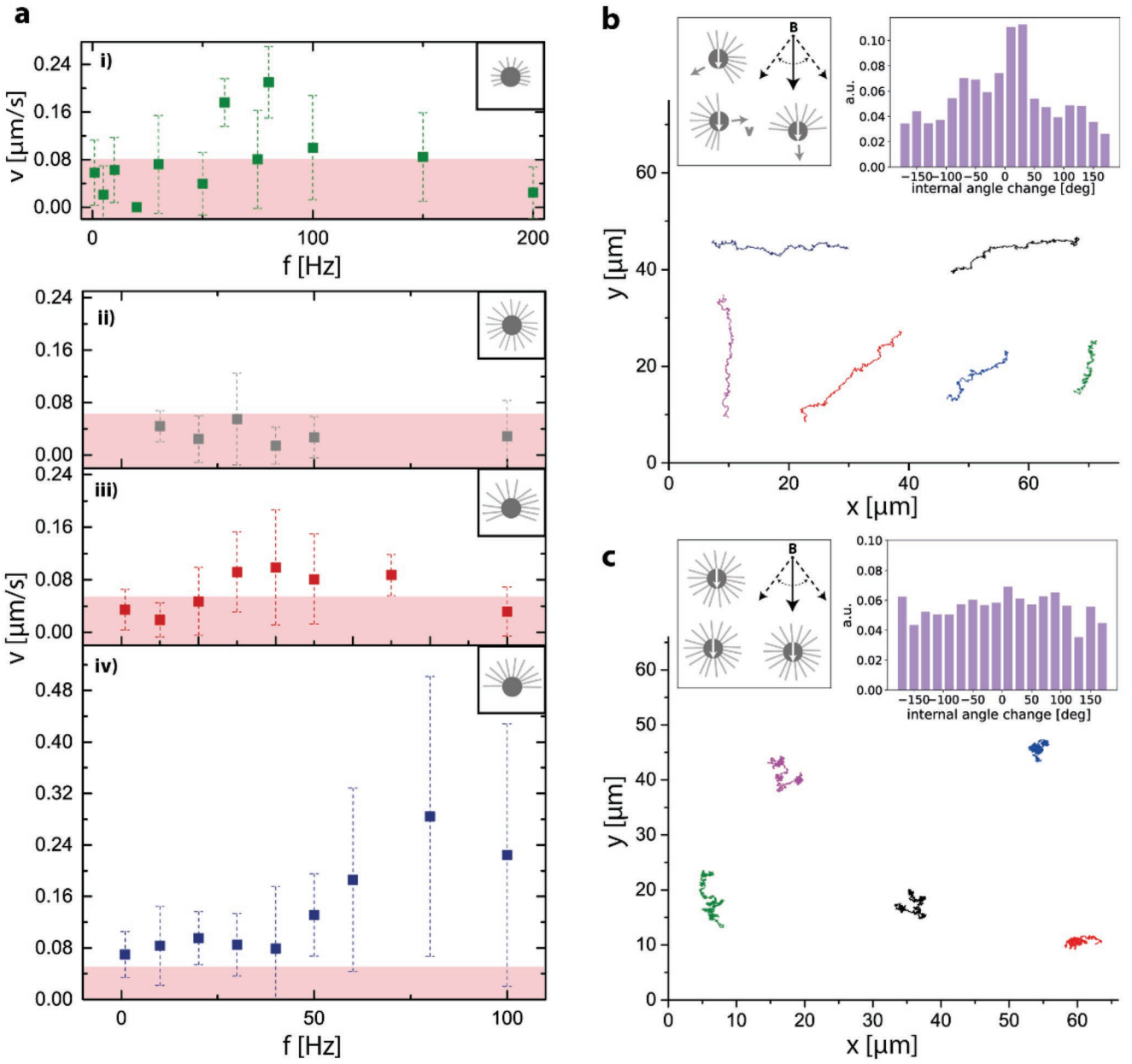

Figure 2. a) Magnetic field frequency, *f*, and average bead velocity, *v*, curves for i) PCM beads, ii) FC beads, iii) PC beads, and iv) HC beads. Each measurement is averaged over 3 to 15 swimmers, and error bars are standard deviation. Red regions on curves indicate maximum drift recorded using MSD analysis in field-off periods before and after experiments in the presence and the absence of the constant portion of the applied magnetic field (see Experimental Section, "Swimming experiments and analysis"). The size of the error bars is due to the polydispersity of the swimmer, stemming from the degree of origami coverage and its magnetic anisotropy b) Tracks of HC beads showing ballistic motion when subjected to an oscillating magnetic field at 70 Hz. c) Tracks of FC beads showing motion consistent with Brownian dynamics when oscillated at 50 Hz. Both trak sets span 60 s. The inset panels in (b) and (c) depict the idealized bead architecture and the distribution of the internal angle of the tracks. A peak centered on 0° suggests ballistic motion and a flat distribution Brownian motion. All tracks originate from the same field of view but have been reorganized in the *x*–*y* frame for image clarity.

TEM micrographs also reveal that grafted batches have a distribution in 6HB bundle coverage (Section S5, Supporting Information). This distribution will lead to bead-to-bead variation in viscous drag, propulsion generation and ultimately performance. Further divergence of action could arise from the random position of the bundles with respect to the beads' easy magnetic axis: thrust, as generated by a bending wave, would transverse zero to a maximum in the *x*–*y* plane as bundle position changes from orthogonal to parallel to said plane, respectively.

In addition to switchable kinetics, we can impart directionality to our 6HB decorated beads through facile adaption to our grafting procedure. Specifically, we better align the magnetic easy axis with that of the bundles by repeating

© 2022 The Authors. Advanced Materials Technologies published by Wiley-VCH GmbH

2365709x, 2022, 12, Downloaded from https://onlinelibrary.wiley.com/doi/10.1002/admt.202200450 by Cochrane Germany, Wiley Online Library on [29/09/2023]. See the Terms and Conditions (https://onlinelibrary.wiley.com/terms-and-conditions) on Wiley Online Library for rules of use; OA articles are governed by the applicable Creative Commons License

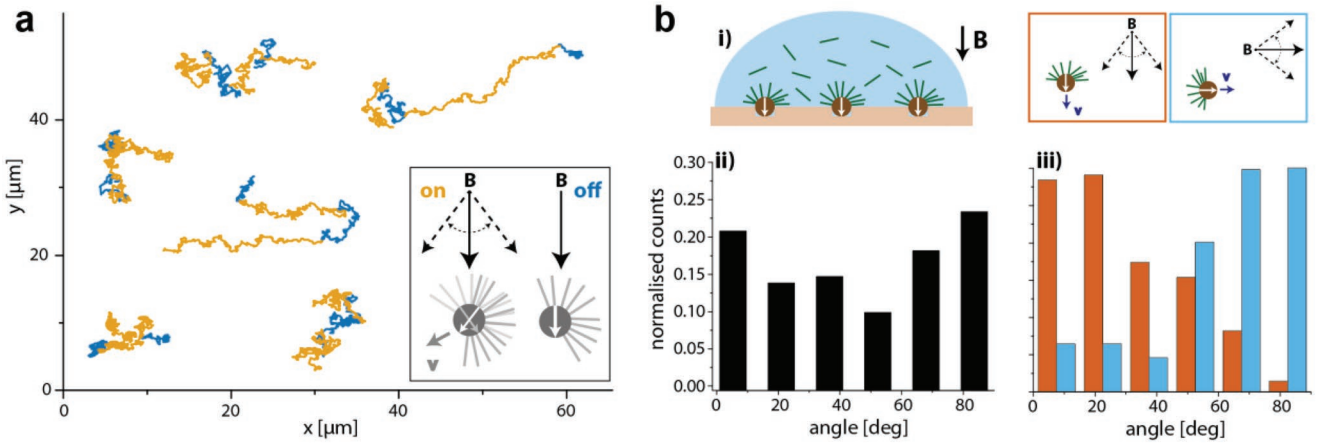

Figure 3. a) Tracks of HC beads on application and removal of an oscillating magnetic field at 60 Hz. Timings are 20 s (off), 60 s (on), 40 s (off), and 60 s (on). The tracks originate from the same field of view but have been reorganized in the *x*–*y* frame for image clarity. b) Magnetically aligned hemispherically covered beads (MAHC). i) Schematic of the preparation of MAHC beads. ii) The angle distribution of vectors spanning the starting and end positions of HC beads with the magnetic field fluctuating around 90° (orange box in (i)) and iii) the vector angle distribution for MAHC beads with a magnetic field fluctuating around 90° and 0°. The histograms were averaged over 68 and 34 beads for the HC and MAHC beads, respectively. Angular symmetries are collapsed to populate a 0–90° range.

the grafting methodology utilized for the HC beads under a 30 mT magnetic field, applied orthogonal to the grafting plane (Figure 3b). The thus formed magnetically aligned HC beads (MAHC beads) locomote predominately along the time-average direction of the fluctuating magnetic field. Furthermore, by rotating said field by |½ π| we induce a ±½ π directional change to their path (Figure 3b-iii). Such directionality broadens the application potential of our devices, particularly in the realm of in/ex vivo targeted treatment. Despite their relatively modest top velocities, the devices seem well suited to such a task not only due to their biocompatible nature but because their actuation with homogenous fields permits their long-distance operation as required for in vivo functionality. Moreover, besides providing thrust, the DNA origami bundles can automatically capture and release cyclic drugs and act as vectors for cellular uptake. The addressable nature of DNA origami also provides scope for customized treatments in the future which as far as we are aware is absent in other micromotors.[53–55]

3. Conclusion

To conclude, in this communication, we have outlined a procedure to fabricate magnetic beads decorated with custom-made DNA origami bundles. Employing an adaptive grafting procedure, we can modulate the surface coverage of the beads from full to anisotropically covered. On their magnetic actuation, the dynamics of fully covered beads can be understood by thermal motion alone, whereas the anisotropically covered sets display ballistics dynamics. This ballistic behavior can be explained by the action of the DNA origami bundles as beating appendages to induce swimming on the microscale. There is still much to be understood about our system: primarily, in the picture we have set out, it is still to be elucidated whether the origami bundles beat as individual units or whether they operate collectively as a single large paddle formed by inter bundle entanglements. Nevertheless, looking forward, we note the potential of our micromotors for biocompatible active-agent delivery on the microscale; DNA origami bundles are excellent capture and release reservoirs for a variety of cyclic drugs.[55] Moreover, whilst we have employed the robust and well understood 6HB DNA origami as appendages in this POC work, there is considerable scope for alternative DNA origami designs from which to generate further adaption to and understanding of nano/microscale motion.

4. Experimental Section

Monomers and Dimers Preparation: Briefly, two sets of six helix bundles (6HB) were designed using the Cadnano2 software (https://github.com/douglaslab/cadnano2).[37] The first set was functionalized at one end with biotin, via complementary base pair staples. For end-to-end oligomerization of the bundle sets, a system of empty scaffold regions and complementary single-stranded intrusion staples were employed, and C4-end staples were used to prevent unwanted polymerization (S6). Two C bases were present on the biotin tagged end for the same purpose. Both structures were first folded separately on a linear temperature ramp from 65 to 20 °C for 19 h without the intrusion-end staples and then purified using PEG precipitation.[56] The individual sets of 6HBs were folded at 10 nM concentration of the 8634 scaffold, 10× excess of core staples, and 30× excess of end staples in a buffer containing 1× TE and 18 mM $MgCl_2$. The scaffold was produced in-house, the staples were purchased from Integrated DNA Technologies. The two purified sets of 6HBs were added together 1:1 to dimerize overnight at 37 °C. The dimer product was separated from remnant monomers using a standard gel electrophoresis protocol.

Grafting of DNA Origami Decorated Magnetic Beads: The biotin-functionalized DNA origami structures were grafted onto streptavidin-covered magnetic beads (Invitrogen, Dynabeads MyOne Streptavidin T1, diameter 1 μm) in three distinct ways to make fully covered beads, partially covered beads, and hemispherically covered beads as follows.

Fully Covered Beads: Magnetic beads were mixed in bulk with the 6HBs (bead:6HBs, 1:100) in TAE gel buffer (40 mM Tris, 20 mM acetic acid, 1 mM EDTA, 11 mM $MgCl_2$) and incubated at room temperature

© 2022 The Authors. Advanced Materials Technologies published by Wiley-VCH GmbH

2365709x, 2022, 12, Downloaded from https://onlinelibrary.wiley.com/doi/10.1002/admt.202200450 by Cochrane Germany, Wiley Online Library on [29/09/2023]. See the Terms and Conditions (https://onlinelibrary.wiley.com/terms-and-conditions) on Wiley Online Library for rules of use; OA articles are governed by the applicable Creative Commons License

overnight. The beads were cleaned in TAE gel buffer via 5 cycles of magnetic collection and supernatant removal.

Partially Covered Beads: A 100 µL droplet of diluted Dynabeads (0.005 nM) in 1× TE buffer (10 mM Tris 1 mM EDTA) with 11 mM $MgCl_2$ was deposited on a glass slide and left for one hour to ensure sedimentation of the beads to the glass surface where they remained stuck. After washing 5 times in TAE gel buffer, a further 100 µL droplet of gel buffer with 6HBs (1 nM) was added and incubated at 4°C overnight in a sealed container to avoid evaporation. After grafting, the beads were collected by pipetting TAE gel buffer with 0.1 wt% sodium dodecyl sulfate (Sigma), which promoted their detachment from the glass substrate. The beads were cleaned as before.

Hemispherically Covered Beads: Here, Dynabeads were prepared at 40 vol% in a solution of SDS-saturated glycerol (distilled water (15 vol%) and glycerol (30 vol%)). The as-produced viscous dispersion was gently wiped over a PDMS mold holding oval microwells with a long (short) axis of 3 µm (2 µm) and well depth of ≈2 µm to leave each well populated with a single bead. The mold was fabricated following standard soft lithographical procedures. The grafting and cleaning protocol of the partially covered beads' system was then repeated.

To align the magnetic easy axis of the beads with the bundles the grafting procedure was repeated in the presence of a 30 mT field aligned with the vertical axis of the mold.

A full description of the above methods employed can be found in Section S6, Supporting Information.

Swimming Experiments and Analysis: After loading the beads in a sealed optical cell, measurements were performed on a Zeiss Axiovert, 100M hal microscope mounted with a pair of oppositely positioned NdFeB disc magnets (35 mm diameter, height 3 mm, superparamagnete) orthogonal to an oppositely positioned pair of magnetic coils (inner diameter 35 mm, outer diameter 57 mm, height 15 mm, 120 turns with 0.85 mm Cu wire, Express Transformers) with a surface-to-surface separation of 75 mm and 30 mm, respectively. To induce motion, a sinusoidal homogenous magnetic field was applied by the coil pair via a function generator (Agilent, 372 33220A) routed through a 200 W power supply (Kepco BOP20-10DL-802E). The following time-varied field was used: $B(t) = B_y + B_x(t))$ where $B_y = 15$ mT was a constant field in the y-direction and $B_x = B_m \sin((f/2\pi)t)$ with $B_m = 7$ mT.

Bead kinetics were recorded with a Thorlabs CMOS Camera (Thorlabs Kiralux CS895CU) using 20× objective at either 5 fps or 32.6 fps. ImageJ's tracking add-on, TrackMate, was employed to extract the tracks from which the mean square displacement, velocity, and internal angle for each particle was calculated with a custom Python script.[57]

Supporting Information

Supporting Information is available from the Wiley Online Library or from the author.

Acknowledgements

The authors would like to thank the German Research Foundation (DFG) for funding under projects TA 1375/1-1 and SFB1032 "Nanoagents," Project A6. MD has received funding from the European Union's Horizon 2020 research and innovation program under the Marie Skłodowska-Curie Grant Agreement No. 765703. The authors would also like to thank Helena Massana-Cid and Carlos Calero Borallo for advice and stimulating discussion.

Open access funding enabled and organized by Projekt DEAL.

Conflict of Interest

The authors declare no conflict of interest.

Authors Contribution

A.V. and C.P. contributed equally to this work. A.V., C.P., and J.T. performed experiments, analyzed results, and contributed to manuscript production. M.D. advised with DNA Origami design. J.T. and T.L. supervised work and conceptualized experiments.

Data Availability Statement

The data that support the findings of this study are available from the corresponding author upon reasonable request.

Keywords

biofabrication, DNA origami, drug delivery, Janus particles, microrobotics, microswimmers, self-assembly

Received: March 19, 2022
Revised: May 13, 2022
Published online: July 24, 2022

[1] G. Gompper, R. G. Winkler, T. Speck, A. Solon, C. Nardini, F. Peruani, H. Löwen, R. Golestanian, U. B. Kaupp, L. Alvarez, T. Kiørboe, E. Lauga, W. C. K. Poon, A. DeSimone, S. Muiños-Landin, A. Fischer, N. A. Söker, F. Cichos, R. Kapral, P. Gaspard, M. Ripoll, F. Sagues, A. Doostmohammadi, J. M. Yeomans, I. S. Aranson, C. Bechinger, H. Stark, C. K. Hemelrijk, F. J. Nedelec, T. Sarkar, et al., *J. Phys.: Condens. Matter* **2020**, *32*, 193001.
[2] M. Fernández-Medina, M. A. Ramos-Docampo, O. Hovorka, V. Salgueiriño, B. Städler, *Adv. Funct. Mater.* **2020**, *30*, 1908283.
[3] Z. Wu, J. Troll, H.-H. Jeong, Q. Wei, M. Stang, F. Ziemssen, Z. Wang, M. Dong, S. Schnichels, T. Qiu, P. Fischer, *Sci. Adv.* **2018**, *4*, eaat4388.
[4] U. Bozuyuk, O. Yasa, I. C. Yasa, H. Ceylan, S. Kizilel, M. Sitti, *ACS Nano* **2018**, *12*, 9617.
[5] P. Illien, R. Golestanian, A. Sen, *Chem. Soc. Rev.* **2017**, *46*, 5508.
[6] L. Schwarz, M. Medina-Sánchez, O. G. Schmidt, *Appl. Phys. Rev.* **2017**, *4*, 031301.
[7] J. Elgeti, R. G. Winkler, G. Gompper, *Rep. Prog. Phys.* **2015**, *78*, 056601.
[8] S. Metri, C. Hakan, H. Wenqi, J. Giltinan, M. Turan, S. Yim, D. Eric, *Physiol. Behav.* **2017**, *176*, 139.
[9] B. J. Nelson, I. K. Kaliakatsos, J. J. Abbott, *Annu. Rev. Biomed. Eng.* **2010**, *12*, 55.
[10] M. F. Copeland, D. B. Weibel, *Soft Matter* **2009**, *5*, 1174.
[11] E. Lauga, T. R. Powers, *Rep. Prog. Phys.* **2009**, *72*, 096601.
[12] V. M. Kadiri, J.-P. Günther, S. N. Kottapalli, R. Goyal, F. Peter, M. Alarcón-Correa, K. Son, H.-N. Barad, M. Börsch, P. Fischer, *Eur. Phys. J. E* **2021**, *44*, 74.
[13] V. Magdanz, I. S. M. Khalil, J. Simmchen, G. P. Furtado, S. Mohanty, J. Gebauer, H. Xu, A. Klingner, A. Aziz, M. Medina-Sánchez, O. G. Schmidt, S. Misra, *Sci. Adv.* **2020**, *6*, eaba5855.
[14] M. R. Bailey, F. Grillo, N. D. Spencer, L. Isa, *Adv. Funct. Mater.* **2022**, *32*, 2109175.
[15] C. Pauer, O. du Roure, J. Heuvingh, T. Liedl, J. Tavacoli, *Adv. Mater.* **2021**, *33*, 2006237.
[16] D. Ahmed, C. Dillinger, A. Hong, B. J. Nelson, *Adv. Mater. Technol.* **2017**, *2*, 1700050.
[17] F. Martinez-Pedrero, H. Massana-Cid, P. Tierno, *Small* **2017**, *13*, 1603449.

© 2022 The Authors. Advanced Materials Technologies published by Wiley-VCH GmbH

2365709x, 2022, 12, Downloaded from https://onlinelibrary.wiley.com/doi/10.1002/admt.202200450 by Cochrane Germany, Wiley Online Library on [29/09/2023]. See the Terms and Conditions (https://onlinelibrary.wiley.com/terms-and-conditions) on Wiley Online Library for rules of use; OA articles are governed by the applicable Creative Commons License

[18] A. Kaiser, A. Snezhko, I. S. Aranson, *Sci. Adv.* **2017**, *3*, e1601469.
[19] M. Driscoll, B. Delmotte, *Curr. Opin. Colloid Interface Sci.* **2019**, *40*, 42.
[20] F. Qiu, B. J. Nelson, *Engineering* **2015**, *1*, 21.
[21] H. Massana-Cid, F. Meng, D. Matsunaga, R. Golestanian, P. Tierno, *Nat. Commun.* **2019**, *10*, 2444.
[22] V. Magdanz, S. Sanchez, O. G. Schmidt, *Adv. Mater.* **2013**, *25*, 6581.
[23] D. Gong, J. Cai, N. Celi, C. Liu, W. Zhang, L. Feng, D. Zhang, *Appl. Phys. Lett.* **2019**, *114*, 123701.
[24] H.-W. Huang, F. E. Uslu, P. Katsamba, E. Lauga, M. S. Sakar, B. J. Nelson, *Sci. Adv.* **2019**, *5*, eaau1532.
[25] R. Dreyfus, J. Baudry, M. L. Roper, M. Fermigier, H. A. Stone, J. Bibette, *Nature* **2005**, *437*, 862.
[26] A. M. Maier, C. Weig, P. Oswald, E. Frey, P. Fischer, T. Liedl, *Nano Lett.* **2016**, *16*, 906.
[27] P. Liao, L. Xing, S. Zhang, D. Sun, *Small* **2019**, *15*, 1901197.
[28] B. Jang, E. Gutman, N. Stucki, B. F. Seitz, P. D. Wendel-García, T. Newton, J. Pokki, O. Ergeneman, S. Pané, Y. Or, B. J. Nelson, *Nano Lett.* **2015**, *15*, 4829.
[29] J. Ali, U. K. Cheang, J. D. Martindale, M. Jabbarzadeh, H. C. Fu, M. Jun Kim, *Sci. Rep.* **2017**, *7*, 14098.
[30] S. F. Schoeller, E. E. Keaveny, *J. R. Soc. Interface* **2018**, *15*, 20170834.
[31] J. Yan, H. Monaco, J. B. Xavier, *Annu. Rev. Microbiol.* **2019**, *73*, 293.
[32] S. F. Schoeller, W. V. Holt, E. E. Keaveny, *Phil. Trans. R. Soc. B* **2020**, *375*, 20190384.
[33] H. S. Fisher, H. E. Hoekstra, *Nature* **2010**, *463*, 801.
[34] C. E. Castro, F. Kilchherr, D.-N. Kim, E. L. Shiao, T. Wauer, P. Wortmann, M. Bathe, H. Dietz, *Nat. Methods* **2011**, *8*, 221.
[35] H. Dietz, S. M. Douglas, W. M. Shih, *Science* **2009**, *325*, 725.
[36] P. W. K. Rothemund, *Nature* **2006**, *440*, 297.
[37] S. M. Douglas, A. H. Marblestone, S. Teerapittayanon, A. Vazquez, G. M. Church, W. M. Shih, *Nucleic Acids Res.* **2009**, *37*, 5001.
[38] S. M. Douglas, J. J. Chou, W. M. Shih, *Proc. Natl. Acad. Sci. U. S. A.* **2007**, *104*, 6644.
[39] D. J. Kauert, T. Kurth, T. Liedl, R. Seidel, *Nano Lett.* **2011**, *11*, 5558.
[40] S. M. Douglas, H. Dietz, T. Liedl, B. Högberg, F. Graf, W. M. Shih, *Nature* **2009**, *459*, 414.
[41] A. Herms, K. Günther, E. Sperling, A. Heerwig, A. Kick, F. Cichos, M. Mertig, *Phys. Status Solidi A* **2017**, *214*, 1600957.
[42] S. Lauback, K. R. Mattioli, A. E. Marras, M. Armstrong, T. P. Rudibaugh, R. Sooryakumar, C. E. Castro, *Nat. Commun.* **2018**, *9*, 1446.
[43] E. Kopperger, J. List, S. Madhira, F. Rothfischer, D. C. Lamb, F. C. Simmel, *Science* **2018**, *359*, 296.
[44] B. Shen, V. Linko, H. Dietz, J. J. Toppari, *Electrophoresis* **2015**, *36*, 255.
[45] F. Kroener, L. Traxler, A. Heerwig, U. Rant, M. Mertig, *ACS Appl. Mater. Interfaces* **2019**, *11*, 2295.
[46] M. M. van Oene, L. E. Dickinson, F. Pedaci, M. Köber, D. Dulin, J. Lipfert, N. H. Dekker, *Phys. Rev. Lett.* **2015**, *114*, 218301.
[47] X. J. A. Janssen, A. J. Schellekens, K. van Ommering, L. J. van IJzendoorn, M. W. J. Prins, *Biosens. Bioelectron.* **2009**, *24*, 1937.
[48] M. J. Saxton, in *Methods in Membrane Lipids* (Ed: A. M. Dopico), Humana Press, Totowa, NJ **2007**, pp. 295–321.
[49] E. Gauger, H. Stark, *Phys. Rev. E – Stat., Nonlinear, Soft Matter Phys.* **2006**, *74*, 021907.
[50] M. Roper, J. Baudry, M. Fermigier, J. Bibette, H. A. Stone, *Proc. R. Soc. A* **2008**, *464*, 877.
[51] G. Taylor, *Proc. R. Soc. London A* **1951**, *209*, 447.
[52] L. Kong, N. F. Rosli, H. L. Chi, J. Guan, M. Pumera, *Bull. Chem. Soc. Jpn.* **2019**, *92*, 1754.
[53] Q. Jiang, S. Liu, J. Liu, Z. Wang, B. Ding, *Adv. Mater.* **2019**, *31*, 1804785.
[54] Q. Jiang, C. Song, J. Nangreave, X. Liu, L. Lin, D. Qiu, Z.-G. Wang, G. Zou, X. Liang, H. Yan, B. Ding, *J. Am. Chem. Soc.* **2012**, *134*, 13396.
[55] H. Ijäs, B. Shen, A. Heuer-Jungemann, A. Keller, M. A. Kostiainen, T. Liedl, J. A. Ihalainen, V. Linko, *Nucleic Acids Res.* **2021**, *49*, 3048.
[56] E. Stahl, T. G. Martin, F. Praetorius, H. Dietz, *Angew. Chem., Int. Ed.* **2014**, *53*, 12735.
[57] J.-Y. Tinevez, N. Perry, J. Schindelin, G. M. Hoopes, G. D. Reynolds, E. Laplantine, S. Y. Bednarek, S. L. Shorte, K. W. Eliceiri, *Methods* **2017**, *115*, 80.

© 2022 The Authors. Advanced Materials Technologies published by Wiley-VCH GmbH

2365709x, 2022, 12, Downloaded from https://onlinelibrary.wiley.com/doi/10.1002/admt.202200450 by Cochrane Germany, Wiley Online Library on [29/09/2023]. See the Terms and Conditions (https://onlinelibrary.wiley.com/terms-and-conditions) on Wiley Online Library for rules of use; OA articles are governed by the applicable Creative Commons License